Utilizing the eikonal relationship in strategies for reentrant wave termination in excitable media

Marcel Hörning,[1,*] Akihiro Isomura,[2] Zhiheng Jia,[3] Emilia Entcheva,[3] and Kenichi Yoshikawa[1,4,†]
[1]*Department of Physics, Graduate School of Science, Kyoto University, Kyoto, Japan*
[2]*Institute for Virus Research, Kyoto University, Kyoto 606-8501, Japan*
[3]*Department of Biomedical Engineering, State University of New York–Stony Brook, Stony Brook, New York 11794, USA*
[4]*Spatio-Temporal Project, ICORP JST, Kyoto 606-8502, Japan*
(Received 24 December 2009; published 12 May 2010)

Obstacle-anchored vortices can be terminated by the application of high-frequency wave trains in excitable media. We theoretically derived the dependency between the obstacle radius and the maximum unpinning period through reinterpretation of the well-known eikonal equation. Our theoretical result was confirmed by experiments with cardiomyocyte monolayers. This result may be useful for improving the stimulation protocol of implantable cardiac pacemakers.

DOI: 10.1103/PhysRevE.81.056202 PACS number(s): 05.45.−a, 87.18.Hf, 87.19.Hh

I. INTRODUCTION

Spiral waves are observed in diverse physical, chemical, and biological systems [1]. The heart has been recognized as one of the main systems in which spiral waves occur, in which such waves can have fatal effects. Spiral waves in the heart, known as ventricular tachycardia (VT), are a precursor of ventricular fibrillation, which is one of the most prevalent diseases in the world. To date, most research has been directed toward elucidating the origin of the formation of VT [2,3]. However, it is still poorly understood how to terminate spiral waves anchored to heterogeneities (blood vessels, scar tissue, etc.), which can easily occur under certain circumstances [4]. Recent papers have proposed various mechanisms [5–7]. Termination by high-frequency stimulation, also known as antitachicardia pacing (ATP), seems to be one of the most promising methods since it is already applied in cardiac pacemakers (defibrillators). While the application of ATP is quite successful, a failure rate of about 10% implies that the therapeutic efficacy should be improved [8].

Free rotating spirals can be easily terminated by the application of high-frequency wave trains. The applied stimulation period needs to be lower than the spiral period. The approaching pacing waves lead to displacement of the spiral core and finally to annihilation at the boundary of the system [9]. However, pinned spiral waves do not necessarily follow this simple framework. It has been shown that weakly anchored spiral waves can be terminated by the delivery of a high-frequency wave train, if the spiral core is larger than the heterogeneity ("obstacle") and the pacing frequency is much higher than the frequency of the free spiral [10]. Excitable waves in the heart are associated with strong dispersion properties, which makes it possible to unpin the rotating wave when the heterogeneity is larger than the spiral core, as has been shown recently [6]. A first approach to explain the necessary conditions was proposed by Tanaka *et al.* [11]. However, this approach is rather complicated and does not clearly explain the essential property of the mechanism. Thus, a simple basic explanation remains to be presented.

The main issue of this paper is that we were able to demonstrate the nature of the termination of a spiral wave that is strongly bound to an obstacle by reinterpreting the well-known eikonal relation (ER) [Eq. (13)] [12,13]. We show that the ER is not only suitable to describing the dispersion relation for wave speed as a function of period, but can also describe the threshold of the pacing period T_p to achieve successful elimination of the pinned spiral wave.

II. NUMERICAL MODEL

To illustrate our arguments, we conducted numerical simulations with the simplified ionic model of heart tissue given by Fenton and Karma [14,15]. Recent papers have shown that this model is suitable for describing features of the heart [6,7]. While this model does not fully account for the rich variety of ionic currents, as do fully ionic models such as the Luo-Rudy model [16], it can fairly well reproduce the action potential of heart cells and mimic important features of heart activity, such as dispersion and restitution properties [14].

The model is based on three main currents through the membrane: the fast inward current J_{fi} and the slow inward and outward currents, J_{si} and J_{so}, respectively. The basic equation for the membrane potential $\mathbf{V}$ is given by

$$\partial_t \mathbf{V} = \boldsymbol{\nabla} \cdot (D \boldsymbol{\nabla} \mathbf{V}) - J_{Ion}(\mathbf{V};\mathbf{v};\mathbf{w})/C_m, \tag{1}$$

where D is the diffusion, C_m is the membrane capacity, $\mathbf{v}$ and $\mathbf{w}$ describe the gating variables, and J_{Ion} is the sum of the three main currents. The membrane potential $\mathbf{V}$ and currents J_{fi}, J_{si}, and J_{so} are scaled by definition to the dimensionless variables $u \equiv (V-V_o)(V_{fi}-V_o)$ and $I \equiv J/[C_m(V_{fi}-V_o)]$, respectively, where V_{fi} is the Nernst potential of the fast inward current and V_o is the resting membrane potential. With the substitution $u_s = u - u_c$, the currents are given as

$$I_{fi} = -\frac{v}{\tau_d}\Theta(u_s)(1-u)(u_s), \tag{2}$$

*Corresponding author. FAX: +81-75-753-3779; marcel@chem.scphys.kyoto-u.ac.jp
†yoshikaw@scphys.kyoto-u.ac.jp

$$I_{si} = \frac{u}{\tau_o}\Theta(-u_s) + \frac{1}{\tau_r}\Theta(u_s), \tag{3}$$

$$I_{so} = -\frac{w}{2\tau_{si}}\{1 + \tanh[k(u - u_c^{si})]\}, \tag{4}$$

where $\Theta(x)$ the Heaviside step function and τ_d are defined as

$$\Theta(x) = \begin{cases} 1, & \text{if } x > 0 \\ 0, & \text{otherwise}, \end{cases} \tag{5}$$

$$\tau_d = C_m / g_{fi}, \tag{6}$$

respectively. The model equations are described as

$$\partial_t u = D\,\nabla \cdot (\nabla \mathbf{u}) - I_{fi}(u;v) - I_{si}(u;w) - I_{so}(u), \tag{7}$$

$$\partial_t v = \Theta(-u_s)(1-v)/\tau_v^-(u) - \Theta(u_s)v/\tau_v^+, \tag{8}$$

$$\partial_t w = \Theta(-u_s)(1-w)/\tau_w^- - \Theta(u_s)w/\tau_w^+, \tag{9}$$

with

$$\tau_v^-(u) = [\Theta(u - u_v)\tau_{v1}^- + \Theta(u_v - u)\tau_{v2}^-]. \tag{10}$$

The parameters were chosen to be the modified Beeler-Reuter variable set in the original paper by Fenton and Karma [14,15]. The depolarization parameter g_{fi} was set to 2.40 mmho/cm^2 in a two-dimensional (2D) isotropic tissue by using dt=0.02 ms and dx=0.016 cm for time and space discretization. The size of the simulated medium was chosen to be 8×8 cm^2, which corresponds to 500×500 lattices points. The system was solved by using a two-dimensional alternating direction implicit scheme. To simulate the obstacle, a circular area in the tissue was disconnected electrically by defining a nonflux boundary condition, corresponding to Neumann boundary condition [17]. The stimuli were applied 5.2 cm from the obstacle center by setting the local membrane potential to +15 mV.

III. RESULTS

A high-frequency wave train is needed to unpin the spiral wave from an obstacle [6]. Therefore, we first focused on the restitution properties of obstacle paced waves. We numerically obtained the restitution curve of 2D-propagating wave trains as illustrated in Fig. 1(a) as a solid blue line with a critical conduction velocity (CV) v_{crit} at a pacing period T_{crit}. Furthermore, we obtained restitution curves on round obstacles by electronically disconnecting an obstacle in finger form (half-circle and rectangle of the same width) with radius R, as illustrated in Fig. 1(c), and initiating wave trains with period T on the upper side of the finger. The CVs obtained for obstacles of different sizes led to a decrease in the CV, as shown by dotted blue lines for obstacles with radii of 1.5, 1.0, 0.5, and 0.4 cm. The pinned spiral wave detached from the obstacle when the critical CV v_p was reached at periodic pacing T_p. The critical CVs obtained, $v_p(T_p,R)$, are plotted with blue plus signs in Fig. 1(a). A schematic illustration is shown in Fig. 1(b) along with definitions of the introduced parameters.

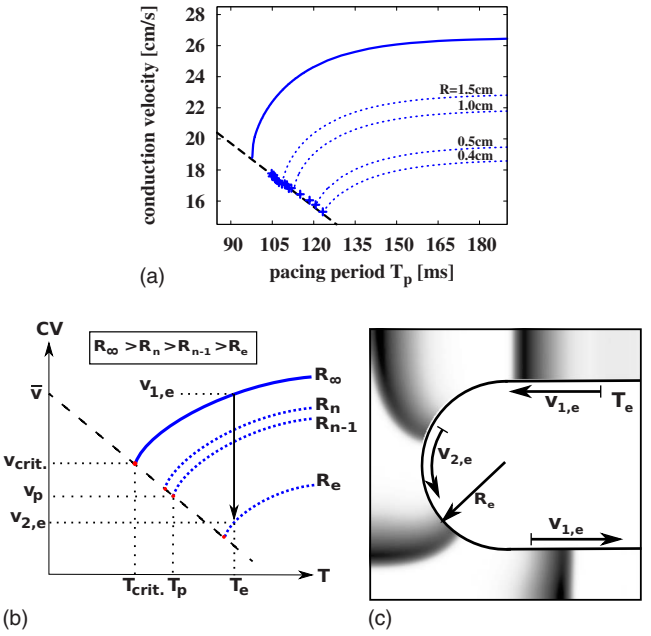

FIG. 1. (Color online) Restitution curves for a round obstacle. (a) The solid blue line is a restitution curve of 2D-plane paced waves. The dotted blue lines are restitution curves of waves on an obstacle with radius R. Critical CVs, v_p, of the restitution curves of obstacles are marked by blue plus signs for radii between 2.1 and 0.4 cm. The dashed black line is the fit of $v_p(T_p,R)$. (b) Illustration of the linear dependency of $v_p(T_p,R)$. An example is given in (c), where a wave train with period T_e is stimulated. Plane waves with CV $v_{1,e}$ propagate toward the round obstacle with radius R_e on the upper plane side, start to curl, reduce the CV to $v_{2,e}$, and finally accelerate back to $v_{1,e}$ on the lower plane side. The change in CV is indicated by a black arrow in (b).

If we assume that the dependency of $v_p(T_p,R)$ is linear, we obtain the following relation:

$$\frac{\bar{v} - v_{crit}}{T_{crit}} = \frac{\bar{v} - v_p}{T_p}, \tag{11}$$

where the indices "*crit*" and "*p*" define the critical speed and pacing period of plane waves and waves propagating on the obstacle, respectively. Further, $\bar{v}$ is the virtual CV where the linear slope crosses the y axis, which defines the slope of the linear decaying critical wave speed for decaying radii [see dashed black line in Figs. 1(a) and 1(b)], which leads to

$$v_p = \frac{T_p}{T_{crit}}(v_{crit} - \bar{v}) + \bar{v}. \tag{12}$$

We now recall the ER to include the effect of curvature in Eq. (12). In two dimensions, the wave speed c for wave fronts with curvature κ can be approximated by [13]

$$c = c_0 + hD\kappa, \tag{13}$$

where c_0 is the normal velocity, D is the diffusion constant, and h is a coefficient [18]. The sign of κ depends on whether the wave is convex (−) or concave (+) around a curve with radius R. Generally, Eq. (13) is only valid for small curvatures and becomes nonlinear in κ when $\kappa \ll c_0/D$ is not ful-

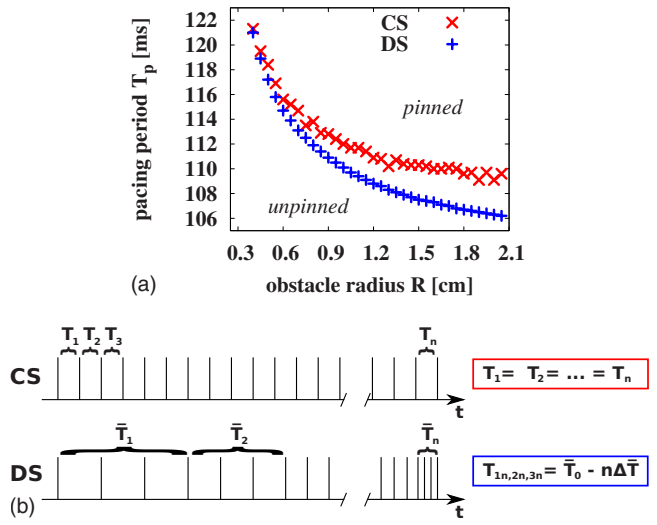

FIG. 2. (Color online) Phase diagram of the termination of a pinned spiral wave. The maximum unpinning period, T_p, at which the unpinning of a pinned spiral wave on an obstacle with radius R, is possible for CS and DS is given in red crosses and blue plus signs, respectively. Above and beneath each curve the spiral wave is still *pinned* and *unpinned*, respectively, after the application of stimulation. CS and DS are illustrated below.

filled. If we assume that the tip of the pinned spiral wave has the same curvature as the obstacle at the critical unpinning speed, $v_p(T_p,R)$, we reconsider Eq. (13) to be

$$v_p(T_p,R) = v_{crit}(T_{crit}) - \frac{D}{R}, \tag{14}$$

where h is assumed to be unity, considering the Zykov limit [18]. Substitution of Eq. (12) into Eq. (14) leads to the maximum pacing period to unpin a spiral wave,

$$T_p = T_{crit}\left(1 + \frac{D}{R(\bar{v} - v_{crit})}\right). \tag{15}$$

To validate Eq. (15), we considered two stimulation protocols: constant stimulation (CS) and dynamical stimulation (DS). When paced with CS, the pacing period T was set constant throughout the entire duration of pacing. On the other hand, when paced with DS, the pacing period was initially set to be $\bar{T}_0$, which is much higher then the maximum unpinning period $T_p(R)$ of CS. The pacing period was then decreased by 0.1 ms on every three applied stimuli (see also the sketch in Fig. 2). This has the advantage that initial alternating waves can entrain before T_p of CS is reached, so that the maximum unpinning period can be obtained reflecting the curvature effect of propagating waves on the obstacle. The spiral wave was defined as unpinned when the spiral wave was liberated from the obstacle and finally terminated on the boundary of the tissue.

Figure 2 shows a phase diagram of the obstacle radii and the maximum unpinning period for the termination of obstacle-anchored spiral waves. The difference in T_p between the stimulation schemes is due to the change in the action-potential duration of the initially paced waves in the

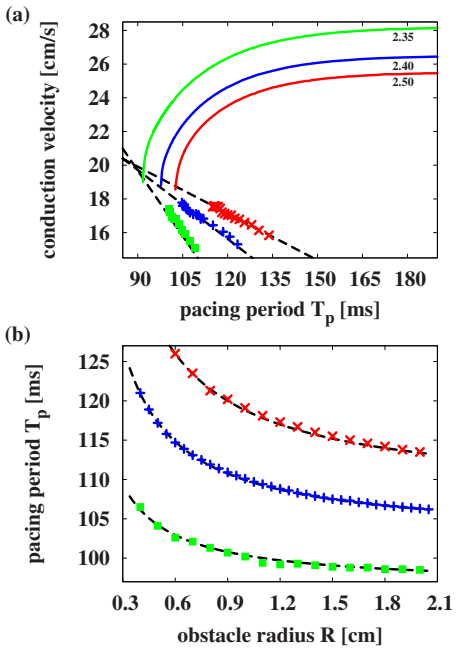

FIG. 3. (Color online) Numerical results for the maximum unpinning period. (a) Restitution curves for g_{fi} values of 2.35, 2.40, and 2.50 mmho/cm^2 shown in solid green, blue, and red lines, respectively. Critical pacing periods are shown as squares, plus signs, and crosses in the respective color for radii of 0.4–2.1 mm in steps of 0.1 mm. The slope of Eq. (12) is shown in dashed black lines for each g_{fi} parameter. (b) The phase diagram of the maximum unpinning period, T_p, for the three g_{fi} parameters in the same color scheme as in (a). Equation (15) is plotted in dashed black lines.

CS scheme. T_p merges for the CS and DS schemes for smaller obstacles since the rotational period of spiral waves is higher for smaller obstacles. This leads to the annihilation of alternating waves apart from the obstacle, so that already or almost pacing-period entrained waves reach the obstacle. On the other hand by applying the DS scheme the pacing waves entrain almost fully before the critical pacing period is reached on the obstacle, so that the effect of alternation is mainly suppressed. This results in a smaller T_p.

To validate the CS and DS schemes, Eq. (15) was fitted to both curves and T_{crit} was calculated. The critical pacing period of 2D-propagating waves was measured to be T_{crit}^{rest} =97.7 ms for the restitution curve shown in Fig. 1(a), whereas T_{crit} was determined to be T_{crit}^{CS}=106.3 ms and T_{crit}^{DS}=102.6 ms, for CS and DS, respectively. T_{crit}^{DS} approximates T_{crit}^{DS} better than T_{crit}^{CS}. The values are not equal since even when the pacing period is decreased in steps of $\Delta\bar{T}$ =0.1 ms, this can induce alternating effects on the obstacle and lead to early unpinning. To obtain $T_{crit}^{rest}=T_{crit}^{DS}$ the pacing step needs to be decreased to $\Delta\bar{T}\to 0$ ms or more than three subsequent constant stimuli need to be chosen. The DS scheme is used below in this paper since it better approximates T_{crit}.

Figures 3(a) and 3(b) show the application of Eqs. (12) and (15), respectively. Three different g_{fi} parameters were chosen to show the generality of the equations. Figure 3(a) shows Eq. (12) as the linear dependency of T_{crit} for different

TABLE I. Table of parameters for different g_{fi}.

g_{fi} (mmho/cm^2)	T_{crit} (ms)	v_{crit} (cm/s)	$\bar{v}$ (cm/s)
2.35	108.0	18.6	28.6
2.40	102.6	18.8	32.8
2.50	96.5	19.0	44.0

g_{fi} parameters in dashed black lines, and approximates T_{crit} of the numerical data very well. With the information obtained regarding $\bar{v}$, and the known T_{crit} and v_{crit} of the restitution curve of plane propagating waves, Eq. (15) is plotted in Fig. 3(b) with the obtained maximum unpinning periods $T_p(R)$. Equation (15) agrees very well with the numerical data. The values for each parameter are summarized in Table I.

Figure 4 illustrates the critical velocity versus the curvature of the obstacle for different excitabilities, where each colored point corresponds to that in Fig. 3. Each excitability approximates the slope of −1 as indicated with black line, which verifies the assumption that the Zykov limit [18] ($h=1$) in Eq. (14) can be adapted.

IV. EXPERIMENTAL RESULTS

Experiments were performed on cardiomyocyte tissue culture to demonstrate the generality of the proposed mechanism and the applicability of Eqs. (12) and (15). Neonatal rat cardiomyocytes were cultured on 22 mm glass coverslips to form confluent monolayers [19]. Obstacles were made of polydimethylsiloxane (PDMS) with a radius between 0.3 and 3 mm, and placed on a glass coverslip before culture. Observations were performed on day 4 on culture by the optical mapping of intracellular calcium using the fluorescent dye Fluo-8. Before the observation, the medium was replaced with Tyrode solution which contained 34 μM lidocaine, a sodium-channel blocker, to decrease the wave speed [6,20]. The tissue was stimulated at its border by a bipolar electrode

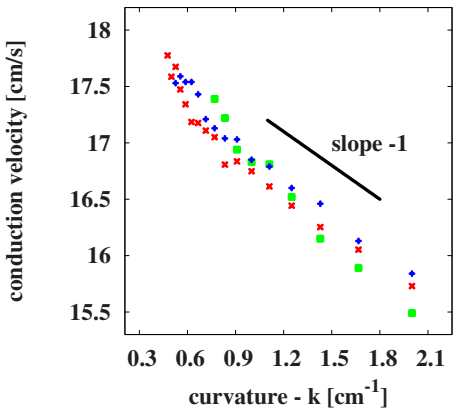

FIG. 4. (Color online) Obstacle curvature of critical velocities. The dependencies of g_{fi} values of 2.35, 2.40, and 2.50 mmho/cm^2 are shown as green squares, blue plus signs, and red crosses, respectively. The black solid line represents the slope of −1.

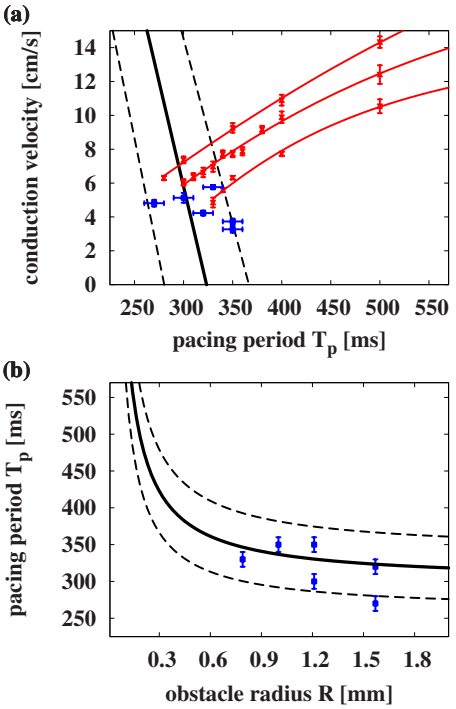

FIG. 5. (Color online) Experimental results with cardiomyocyte monolayers. (a) T_p and the respective v_p of successful unpinning shown in blue squares. Red data points and lines show the restitution curves. Equation (12) is plotted by solid and dashed black lines, by approximating $T_{crit}=300\pm40$ ms, respectively, $v_{crit}=5.8$ cm/s and $\bar{v}=122$ cm/s. (b) Phase diagram of the maximum unpinning period, T_p, for obstacles of different sizes. Equation (15) is plotted with the value obtained in (a). The diffusion constant was assumed to be 1.0 cm^2/s.

using biphasic stimuli of 10 V. Data were acquired by an Andor iXon electron multiplying CCD camera, and processed and analyzed by custom-designed plug-ins in ImageJ.

Spiral waves were created by the application of high-frequency stimuli. The introduced free rotating spiral waves meandered in the tissue and eventually attached to the PDMS obstacle. This effect is often observed in two-dimensional heart tissue. It has been reported that, in the more realistic three-dimensional case of pinning, spiral waves behave in a rather complex manner [21]. As the pacing period was decreased in a stepwise manner, the maximum unpinning period T_p was determined with an error of 10 ms. To gain information about the critical velocity and period, three restitution curves were recorded in the absence of obstacles. T_{crit} and v_{crit} were determined when subsequent stimuli do not lead to wave propagation in a Wenckebach manner. That means that of M stimuli only N lead to wave propagation with $N<M$, e.g., 1:2, 1:3, etc. [22]. Obstacles smaller than approximately 0.7 mm led to weakly pinned spiral waves [20] and were not considered since they were likely associated with a different mechanism [10].

Figure 5(a) shows the phase space of the maximum unpinning period T_p obtained in experiments with cardiomyocyte monolayers (see blue data points in Fig. 5). Spirals pinned to obstacles larger than 1.6 mm could not be unpinned by the high-frequency wave train, but due to the vul-

nerable effect. The applied stimuli introduced a pair of free rotating spiral waves leading to unpinning of the pinned spiral wave [7]. Every experiment was performed on separate cardiomyocyte monolayers, which gave an underlying natural variability [20] and hence different restitution curves and different v_{crit} and T_{crit} in each layer, as shown in the three restitution curves in Fig. 5. Since the CV of the approaching waves and the CV on the obstacle were within the same range of errors of the measured CVs, it is difficult to fit Eqs. (12) and (15). However, it indicates that the slope of critical velocities on obstacles has to be very steep. By approximating v_{crit} and T_{crit}, a fairly good fit can be obtained.

Furthermore, the theoretical derived dependency of the experimental result fits in good agreement with the estimate of Fast and Kleber [23], where the critical radius of curvature, at which wave-front curvature significantly affects conduction in isotropic 2D heart tissue, is estimated as $r_c = 152$ μm when the propagating wave speed of a flat wave is approximately 50 cm/s. Our data suggest that the critical radius can be estimated as a few hundred micrometers [see Fig. 5(b)]. This range fits in good agreement since in our experiments lidocaine is used to suppress the wave speed of flat waves to be approximately 20 cm/s, which increases the effect of curvature [23].

V. CONCLUSION

Unpinning a spiral wave by a high-frequency wave train was studied numerically. We have found that the maximum unpinning period to liberate a spiral wave from an obstacle is consistent with a reinterpreted eikonal relation and can be approximated by Eq. (15). Additionally we have shown that the critical velocity of high-frequency wave trains decreases linearly with a decrease in the size of the obstacle.

The unpinning mechanism is summarized briefly as follows. The approaching wave train reduces its speed on the obstacle due to curvature. When the wave speed on the obstacle exceeds the critical velocity, defined by the restitution properties of the obstacle, the waves fail to conduct and detach from the obstacle. Subsequent approaching waves push the detached spiral wave away from the obstacle until it terminates on the boundary of the system.

Our results indicate that the unpinning of an obstacle-anchored spiral wave is determined by the curvature effect and the dispersion and restitution properties of the medium, and this was validated by experiments with two-dimensional heart tissue culture. Different pacing protocols can increase the possibility of successful unpinning. The maximum unpinning period can be increased by applying CS, which reduces the possibility of inducing new spiral waves to the tissue, since the maximum unpinning period is higher than that with the DS scheme, which reduces the possibility of inducing spiral breakups which could lead to fibrillationlike states [24]. This result may improve the efficacy and reliability of cardiac pacemakers in clinical use. Although numerical and experimental results show good agreement, three-dimensional studies will be necessary to provide a full picture of the unpinning process related to real heart applications since additional effects might play an important role such as cell orientation, wave filaments, different obstacle shapes (vessel-like and scarelike), and the pinning effect [21].

ACKNOWLEDGMENTS

The authors thank Dr. Sergii Rudiuk for his helpful discussions. This research was supported in part by JSPS (Grant No. 21-102).

[1] M. C. Cross and P. C. Hochenberg, Rev. Mod. Phys. **65**, 851 (1993).
[2] F. Fenton *et al.*, Chaos **12**, 852 (2002).
[3] B. Echebarria and A. Karma, Phys. Rev. E **76**, 051911 (2007).
[4] A. Pertsov *et al.*, Circ. Res. **72**, 631 (1993).
[5] J. Cysyk and L. Tung, Biophys. J. **94**, 1533 (2008).
[6] A. Isomura, M. Hörning, K. Agladze, and K. Yoshikawa, Phys. Rev. E **78**, 066216 (2008).
[7] M. Hörning, A. Isomura, K. Agladze, and K. Yoshikawa, Phys. Rev. E **79**, 026218 (2009).
[8] A. Schaumann *et al.*, Circulation **97**, 66 (1998).
[9] K. Agladze *et al.*, Am. J. Physiol. Heart Circ. Physiol. **293**, H503 (2007).
[10] A. Pumir, S. Sinha, S. Sridhar, M. Argentina, M. Hörning, S. Filippi, C. Cherubini, S. Luther, and V. Krinsky, Phys. Rev. E **81**, 010901(R) (2010).
[11] M. Tanaka *et al.*, Chaos **19**, 043114 (2009).
[12] C. Cabo *et al.*, Circ. Res. **75**, 1014 (1994).
[13] J. P. Keener, SIAM J. Appl. Math. **6**, 46 (1986).
[14] F. Fenton and A. Karma, Chaos **8**, 1 (1998).
[15] F. Fenton and A. Karma, Chaos **8**, 879 (1998).
[16] C. H. Luo and Y. Rudy, Circ. Res. **68**, 1501 (1991).
[17] Z. Qu *et al.*, Ann. Biomed. Eng. **28**, 755 (2000).
[18] A. M. Pertsov, M. Wellner, and J. Jalife, Phys. Rev. Lett. **78**, 2656 (1997).
[19] S. Matoba *et al.*, Circulation **99**, 817 (1999).
[20] Z. Y. Lim *et al.*, Circulation **114**, 2113 (2006).
[21] Z. A. Jimenez, B. Marts, and O. Steinbock, Phys. Rev. Lett. **102**, 244101 (2009).
[22] H. Bien *et al.*, Biophys. J. **90**, 2628 (2006).
[23] V. G. Fast and A. G. Kleber, Cardiovasc. Res. **33**, 258 (1997).
[24] E. M. Cherry and F. H. Fenton, Am. J. Physiol. **286**, 2332 (2004).